

Proton-proton scattering without Coulomb force renormalization

R. Skibiński, J. Golak, and H. Witała

M. Smoluchowski Institute of Physics,

Jagiellonian University, PL-30059 Kraków, Poland

W. Glöckle

Institut für theoretische Physik II, Ruhr-Universität Bochum, D-44780 Bochum, Germany

(Dated: October 25, 2018)

Abstract

We demonstrate numerically that proton-proton (pp) scattering observables can be determined directly by standard short range methods using a screened pp Coulomb force without renormalization. In examples the appropriate screening radii are given. We also numerically investigate solutions of the 3-dimensional Lippmann-Schwinger (LS) equation for a screened Coulomb potential alone in the limit of large screening radii and confirm analytically predicted properties for off-shell, half-shell and on-shell Coulomb t-matrices. These 3-dimensional solutions will form a basis for a novel approach to include the pp Coulomb interaction into the 3N Faddeev framework.

PACS numbers: 21.45.-v, 21.45.Bc, 25.10.+s, 25.40.Cm

I. INTRODUCTION

The action of the Coulomb force in pp scattering can be rigorously treated using the Vincent-Phatak method [1]. We propose an alternative manner using a screened Coulomb force, despite the well known fact that the screening limit does not exist. Namely the pp on-shell scattering amplitude acquires an oscillating phase factor if the screening radius goes to infinity [2, 3, 4, 5]. This phase factor is known and can be removed, a step known in that context under the name renormalization. However, as we shall show, if one is interested in the pp observables (not in the phase shifts) where that phase factor drops out, all scattering observables can be obtained in the standard framework of short range interactions. This will be demonstrated in section II for suitably chosen screening radii.

In view of a forthcoming paper [6] related to the pd system, we further investigate in section III properties of the screened 3-dimensional Coulomb t-matrix $\langle \vec{p}' | t_c^R(E) | \vec{p} \rangle$. This t-matrix is a solution of the 3-dimensional 2-body LS equation driven by the screened Coulomb potential. Namely to catch the full action of the Coulomb force in the pd system a partial wave truncated pp t-matrix is insufficient and the complete 3-dimensional Coulomb t-matrix has to be used. Analytical properties of that screened Coulomb t-matrix, off-the-energy-shell, half-shell and on-shell have been studied in the past [2, 3, 4, 7, 8]. These investigations, however, mostly rely on insights gained for fixed partial wave states. The mathematical rigor in the summation of the partial wave sum to infinity leaves room for improvement. Therefore we felt that a numerical study is justified to verify statements given there: the screening limit of $\langle \vec{p}' | t_c^R(E) | \vec{p} \rangle$ exists for $\frac{p'^2}{m} \neq E \neq \frac{p^2}{m}$ and coincides with the unscreened pure Coulomb force expression, which is known analytically [2, 9] and references therein; that screening limit exhibits a discontinuity if p approaches $\sqrt{m_p E}$, $E > 0$ from above or below; the screening limit of the on-shell t-matrix $\langle p \hat{p}' | t_c^R(E = \frac{p^2}{m}) | \vec{p} \rangle$ approaches the analytically known unscreened Coulomb on-shell t-matrix up to a given infinitely oscillating phase factor. Here we want to numerically investigate at which R-values these limits are reached with adequate accuracy. We conclude in section IV.

II. THE ON-SHELL PP T-MATRIX WITH SCREENED COULOMB POTENTIAL AND THE PP OBSERVABLES

Let V_c^R be the screened Coulomb potential between 2 protons normalised such that V_c^R turns into the pure pp Coulomb potential for R , the screening radius, going to infinity. Together with

the strong interaction V this determines the 2-body pp t-matrix via the LS equation

$$t = V + V_c^R + (V + V_c^R)G_0t , \quad (1)$$

where G_0 is the free propagator. That equation is solved at the pp c.m. energy $E = \frac{p^2}{m_p}$ projected on a set of partial wave basis states $|p(ls)jm; tm_t\rangle$, with p, l, s, j and m the relative momentum, orbital angular momentum, total spin, total angular momentum and its magnetic quantum number.

The total isospin quantum numbers for two protons are $t = 1$ and $m_t = -1$. This leads to the on-the-energy-shell t-matrix element

$$\langle p(l's')j'm'|t|p(ls)jm \rangle = \delta_{s's}\delta_{j'j}\delta_{m'm}t_{l'l}^{sj}(p, p) , \quad (2)$$

where the Pauli principle dictates $(-)^{l+s} = 1$ and we took s to be conserved.

The full 3-dimensional antisymmetrized on-shell t-matrix is given as

$$\langle \vec{p}'m'_1m'_2|t(1 - P_{12})|\vec{p}m_1m_2 \rangle , \quad (3)$$

where $m_i(m'_i)$ are the individual spin magnetic quantum numbers and $\vec{p} = p\hat{p}$, $\vec{p}' = p\hat{p}'$ the initial and final relative momenta.

The standard partial wave decomposition leads to

$$\begin{aligned} \langle \vec{p}'m'_1m'_2|t(1 - P_{12})|\vec{p}m_1m_2 \rangle &= \sum_s (\frac{1}{2}\frac{1}{2}s, m'_1m'_2m'_s)(\frac{1}{2}\frac{1}{2}s, m_1m_2m_s) \\ &\sum_{j=0}^{\infty} \sum_{m=-j}^j \sum_{l'=|j-s|}^{j+s} \sum_{l=|j-s|}^{j+s} \sum_{m'_l} (l'sj, m'_l, m'_s, m) Y_{l'm'_l}(\hat{p}') t_{l'l}^{sj}(p, p) (1 + (-)^{l+s}) \\ &\sum_{m_l} (lsj, m_l m_s, m) Y_{l'm_l}^*(\hat{p}) . \end{aligned} \quad (4)$$

The strong force can be neglected beyond a certain j_{max} and there only the screened Coulomb t-matrix t_{cl}^R is present, which is diagonal in l and independent of s and j . In a well known manner one adds and subtracts a finite sum up to j_{max} with t_{cl}^R only and this completes the infinite sum over j containing only t_{cl}^R . That infinite sum is identical to the 3-dimensional antisymmetric screened Coulomb t-matrix. Thus (4) turns into

$$\begin{aligned} \langle \vec{p}'m'_1m'_2|t(1 - P_{12})|\vec{p}m_1m_2 \rangle &= \delta_{m'_1m_1}\delta_{m'_2m_2} \langle \vec{p}'|t_c^R|\vec{p} \rangle - \delta_{m'_1m_2}\delta_{m'_2m_1} \langle \vec{p}'|t_c^R| - \vec{p} \rangle \\ &+ \sum_s (\frac{1}{2}\frac{1}{2}s, m'_1m'_2m'_s)(\frac{1}{2}\frac{1}{2}s, m_1m_2m_s) \sum_{j=0}^{\infty} \sum_{m=-j}^j \sum_{l'=|j-s|}^{j+s} \sum_{l=|j-s|}^{j+s} \sum_{m'_l} (l'sj, m'_l, m'_s, m) \\ &Y_{l'm'_l}(\hat{p}') (t_{l'l}^{sj}(p, p) - \delta_{l'l}t_{cl}^R) (1 + (-)^{l+s}) \sum_{m_l} (lsj, m_l m_s, m) Y_{l'm_l}^*(\hat{p}) . \end{aligned} \quad (5)$$

Now as is well known [3, 4] the limit of that expression does not exist for $R \rightarrow \infty$. In that limit each term in (5) acquires the same infinitely oscillating factor $e^{2i\Phi_R(p)}$, where $\Phi_R(p)$ is given below. If one is interested in scattering phase shifts it is unavoidable to keep track of this oscillating factor which in that context runs under the name renormalization [5]. However, if one is interested in the pp observables, the cross section and all sorts of spin observables (note $\Phi_R(p)$ is independent of spin magnetic quantum numbers), where the on-shell t-matrix appears together with its complex conjugate, the oscillating factor drops out. In that case one does not even have to know the analytical form of $\Phi_R(p)$. It is sufficient to know that the limit of large screening radius generates just a phase factor.

This is the main message of this section: the pp observables based on the strong and the screened Coulomb force can be calculated without renormalization using standard short range methods. Though not explicitly stated in [3, 4] this insight is in the spirit of these authors. It remains to establish the values of the parameter R at which the observables get independent of R .

Based on (5) all pp-scattering observables are given by well known analytic expressions [10], here, however, we use a more modern nomenclature for the various spin observables [11]. We use the following screening form which depends on two parameters, the screening radius R and the power n :

$$V_c^R(r) = \frac{e^2}{r} e^{-(\frac{r}{R})^n}. \quad (6)$$

At a given value n the pure Coulomb potential results for $R \rightarrow \infty$. We use $n = 1, 2, 3$, and 4 . As has been shown in [12] based on [3, 4], the related phase $\Phi_R(p)$ is given as

$$\Phi_R(p) = -\eta[\ln(2pR) - \gamma/n] \quad (7)$$

where $\gamma = 0.5772\dots$ is the Euler number and $\eta = \frac{m_p e^2}{2p}$ the Sommerfeld parameter.

Considering only the screened Coulomb force (6) the leading term in (1) is given by

$$\langle \vec{p}' | V_c^R | \vec{p} \rangle = \frac{e^2}{2\pi^2} \frac{1}{|\vec{p} - \vec{p}'|} \int_0^\infty dr \sin(|\vec{p} - \vec{p}'|r) e^{-(\frac{r}{R})^n}. \quad (8)$$

By a simple partial integration it can be shown that this matrix element approaches the n-independent limit

$$\lim_{R \rightarrow \infty} \langle \vec{p}' | V_c^R | \vec{p} \rangle = \frac{e^2}{2\pi^2 |\vec{p} - \vec{p}'|^2}. \quad (9)$$

Therefore for suitably large R -values the leading term and thus the solution of the LS equation (1) will approach a n-independent limit.

In Figs. 1 and 2 we demonstrate at $E_p^{lab} = 13$ MeV for several pp observables independence on n for a suitably large R -value and the perfect agreement to the exact Vincent-Phatak [1] results at $E_p^{lab} = 13$ MeV. The deviation with respect to the standard Vincent-Phatak approach [1], which treats the pp Coulomb force rigorously, for different pp observables and values of $n = 1, 2, 3$ and 4 and screening radius $R = 120$ fm is under $\approx 1\%$.

In Figs. 3 and 4 we show the convergence with respect to R for $n = 4$ for a number of pp observables at $E_p^{lab} = 13$ MeV. The corresponding results for $E_p^{lab} = 50$ MeV are shown in Figs. 5 and 6. The resulting limiting values agree very well with the Vincent-Phatak results. At $E_p^{lab} = 13$ MeV the limiting R -value is $R = 120$ fm and at $E_p^{lab} = 50$ MeV $R = 60$ fm. With decreasing energy the limiting R -value increases.

III. PROPERTIES OF THE 3-DIMENSIONAL SCREENED COULOMB T-MATRIX

As will be shown in a forthcoming article [6] the 3-dimensional screened pp Coulomb t-matrix $\langle \vec{p}' | t_c^R(E) | \vec{p} \rangle$ occurs naturally in a certain type of Faddeev equation of the pd scattering problem. There it appears off-the-energy-shell (with the exception of isolated points). For the unscreened pure Coulomb force the off-the-energy-shell expression is analytically known [2, 9].

We numerically investigate the screening limits of $\langle \vec{p}' | t_c^R(E) | \vec{p} \rangle$ for $\frac{p'^2}{m} \neq E \neq \frac{p^2}{m}$ (off-shell), for $p' \neq p$ and $E = \frac{p^2}{m_p}$ (half-shell) and for $p' = p$ and $E = \frac{p^2}{m_p}$ (on-shell). Here we want to numerically investigate at which R -values the limits are reached with adequate accuracy and how they are related to the corresponding unscreened pure Coulomb force expressions.

To that aim we regard the LS equation for two protons interacting only with the screened Coulomb potential V_c^R . The off-shell t-matrix element $\langle \vec{p}' | t_c^R(E = \frac{k^2}{m_p}) | \vec{p} \rangle \equiv t_c^R(p', p, x = \hat{p} \cdot \hat{p}'; E)$ fulfills for given energy E the equation [13]

$$t_c^R(p', p, x) = \frac{1}{2\pi} v_c^R(p', p, x, 1) + \int_0^\infty dp'' p''^2 \int_{-1}^1 dx'' v_c^R(p', p'', x, x'') \frac{1}{E + i\epsilon - \frac{p''^2}{m_p}} t_c^R(p'', p, x'') \quad (10)$$

with

$$v_c^R(p', p, x', x) \equiv \int_0^{2\pi} d\phi V_c^R(p', p, x' x + \sqrt{1-x'^2} \sqrt{1-x^2} \cos\phi) . \quad (11)$$

Eq. (10) can be solved after discretizing x and the continuous momentum variables using direct matrix inversion or generating the Neumann series and applying Padè summation.

We solved (10) at three energies: $E = 3$ MeV, 13 MeV, and 50 MeV. For $n = 1$ the leading

term in (10) can be calculated analytically

$$v_c^R(p', p, x', x) = \frac{e^2}{\pi \sqrt{(p'^2 + p^2 - 2p'px'x + \frac{1}{R^2})^2 - 4p'^2p^2(1 - x'^2)(1 - x^2)}}. \quad (12)$$

For $n > 1$ this is no more possible and a two-dimensional numerical integration is required to get the leading term

$$v(p', p, x', x) = \frac{e^2}{2\pi^2} \int_0^{2\pi} d\phi \int_0^\infty dr \frac{1}{\sqrt{p^2 + p'^2 - 2pp'(x'x\sqrt{1 - x'^2}\sqrt{1 - x^2}\cos\phi)}} e^{-(\frac{r}{R})^n}. \quad (13)$$

On the other hand the pure off-shell Coulomb t-matrix is known analytically ([2, 9] and references therein)

$$\langle \vec{p}' | t_c^R(\frac{k^2}{m_p}) | \vec{p} \rangle \rightarrow \frac{e^2}{2\pi^2} \frac{1 + I(x)}{(\vec{p}' - \vec{p})^2} \quad (14)$$

with

$$I(x) = \frac{1}{x} [{}_2F_1(1, i\eta; 1 + i\eta; \frac{x+1}{x-1}) - {}_2F_1(1, i\eta; 1 + i\eta; \frac{x-1}{x+1})] \quad (15)$$

and $x^2 = 1 + \frac{(p'^2 - k^2)(p^2 - k^2)}{k^2(\vec{p}' - \vec{p})^2}$. ${}_2F_1$ is the hypergeometric function [14], which we determined using subroutines from [15] and paid attention to the vanishing small positive imaginary part of k^2 .

As an illustration of our general results we show in Fig. 7 the limiting behavior for the real and imaginary parts of the off-shell screened Coulomb t-matrix $t_c^R(p, p', x)$ at $E_p^{lab} = 13$ MeV and fixed p and x values as a function of p' . This energy corresponds to the on-shell momentum $k = 0.396$ fm $^{-1}$. The small R -values $R = 20$ fm and $R = 60$ fm are quite insufficient, especially for the imaginary part, to reach the pure Coulomb off-shell values. For the higher R -values, $R = 120$ fm and beyond, $t_c^R(p, p', x)$ converges very well and the limit coincides, as expected, with the pure Coulomb off-shell t-matrix. For $p' = k = 0.396$ fm $^{-1}$ one reaches the half-shell point and in its neighborhood a discontinuity develops with increasing R -values, if one approaches k from below or above. That discontinuity is very well known to exist for the pure half-shell Coulomb t-matrix and reproduced for the convenience of the reader:

$$t_c(p, p', x, E = \frac{k^2}{m_p}) = \frac{e^2}{2\pi^2} \frac{1}{|\vec{p} - \vec{p}'|^2} \frac{2\pi\eta}{1 - e^{-2\pi\eta}} e^{i\eta \ln \frac{k^2 - p'^2}{4k^2|\vec{p} - \vec{p}'|^2}} e^{i\eta \ln |k^2 - p'^2|} \begin{cases} 1 & k^2 > p'^2 \\ e^{-\pi\eta} & k^2 < p'^2 \end{cases} \quad (16)$$

That discontinuity is separately shown in Fig. 8 for both parts of the pure Coulomb t-matrix, for predictions based on Eqs 14-15. The screened Coulomb t-matrix is, of course, continuous at $p' = k$ for each fixed R -value, but nevertheless the tendency to develop that discontinuity can be seen with increasing R .

Now as has been emphasized in [7, 8] that discontinuity would be absent if the limits $p' \rightarrow k$ and $R \rightarrow \infty$ are performed such that $|p' - k|R \rightarrow 0$. To show that numerically a more subtle investigation is required, which we did not undertake.

Fig. 9 exemplifies the situation for the off-shell t-matrix at negative energy $E_p^{lab} = -13$ MeV, where the t-matrix is real. There the limit is reached already around $R = 20$ fm.

Let us turn now to the half-shell pure Coulomb t-matrix, which is analytically given by [16].

$$\langle \vec{p}' | t_c^R \left(\frac{k^2}{m_p} \right) | \vec{k} \rangle \rightarrow C_0 e^{i\sigma_0} \frac{k\eta}{\pi^2 q^2} \left(\frac{p'^2 - k^2}{q^2} \right)^{i\eta}, \quad (17)$$

where $\vec{q} = \vec{p}' - \vec{k}$ is the momentum transfer, $\sigma_0 = \Gamma(1 + i\eta)$ is the pure Coulomb phase shift and $C_0^2 = \frac{2\pi\eta}{\exp^{2\pi\eta} - 1}$ is the Coulomb penetrability. The direct comparison of this limit and the screened Coulomb half-shell t-matrix is shown in Figs. 10 and 11 for the real and the imaginary part of t at $E_p^{lab} = 13$ MeV, respectively. On both figures, in upper row discrepancy due to the oscillating factor $e^{i\Phi_R(k)}$ [3, 4, 5] is seen. After removing that factor (by procedure called renormalization) the screened half-shell t-matrix approaches in the limit $R \rightarrow \infty$ the half-shell Coulomb t-matrix, what is shown in lower row of Figs. 10 and 11. The results of renormalization are striking, especially for the imaginary part of the half-shell screened t-matrix. The screening radii about $R = 60$ fm is sufficient to describe the pure Coulomb t-matrix, however for smaller angles one has to go even to higher R 's.

Finally let us regard the screened on-the-energy-shell t-matrix element, which acquires for large R -values the oscillating factor $e^{2i\Phi_R(k)}$ [3, 4, 5]. After renormalization with this factor the screened on-the-energy-shell t-matrix approaches in the limit $R \rightarrow \infty$ the Coulomb scattering amplitude $A_C(\theta)$ [5, 17]

$$t_c^R(k, k, x)|_{renormalized} \equiv e^{-2i\Phi_R(k)} t_c^R(k, k, x) \rightarrow -\frac{2}{m_p} \frac{A_C(\theta)}{(2\pi)^2} = \frac{2}{m_p(2\pi)^2} \frac{m_p e^2}{4k^2} \frac{e^{-i\eta \ln(\sin^2 \frac{\theta}{2})}}{\sin^2 \frac{\theta}{2}}. \quad (18)$$

This is demonstrated in Fig. 12 for the real part and in Fig. 13 for the imaginary part of the on-shell t-matrix at $E_p^{lab} = 13$ MeV. The upper rows show unrenormalized screened t-matrices while the lower rows show them after renormalization. It is clearly seen that the renormalization is required to get the Coulomb on-shell amplitude (shown by the thick solid line). The effect of renormalization is very pronounced for the imaginary part. It is negative without renormalization and shows a strong dependence on the screening radii R . After renormalization and for sufficiently large R -values it perfectly overlaps with the imaginary part of the pure Coulomb on-shell amplitude. At forward angles, which corresponds to x close to 1, $R = 180$ fm is required to reach good agreement with the pure on-shell Coulomb t-matrix.

IV. SUMMARY AND OUTLOOK

We numerically solved the 3-dimensional LS equation for a general off-shell screened Coulomb t-matrix with different types of screening. That t-matrix taken on-shell together with a finite number of partial wave projected t-matrices generated by the sum of the screened Coulomb force and the nuclear force and corrected for the partial wave projected screened pure Coulomb t-matrix leads to correct pp observables at suitably chosen finite screening radii. The renormalization phases drop out automatically in the pp observables since they are products of the full t-matrix and its complex conjugate. Thus renormalization is not required and even the knowledge of the renormalization phase is not required when calculating observables.

Finally we numerically checked that the screened 3-dimensional Coulomb t-matrix has the off-shell, half-shell and on-shell limits in relation to the general unscreened pure Coulomb t-matrix, which have been analytically predicted in the literature. We felt that this numerical 3-dimensional investigation supplements well those previous analytical studies, which lack mathematical rigor when summing partial wave results to infinite order.

The resulting 3-dimensional screened general Coulomb t-matrix will be used in a forthcoming Faddeev treatment of pd reactions.

Acknowledgments

This work was supported by the 2008-2011 Polish science funds as a research project No. N N202 077435. It was also partially supported by the Helmholtz Association through funds provided to the virtual institute “Spin and strong QCD”(VH-VI-231) and by the European Community-Research Infrastructure Integrating Activity “Study of Strongly Interacting Matter” (acronym HadronPhysics2, Grant Agreement n. 227431) under the Seventh Framework Programme of EU. The numerical calculations were performed on the supercomputer cluster of the JSC, Jülich, Germany.

- [1] C. M. Vincent and S. C. Phatak, Phys. Rev. **C10**, 391 (1974).
- [2] J.C.Y. Chen and A.C. Chen, in Advances of Atomic and Molecular Physics, edited by D. R. Bates and J. Estermann (Academic, New York, 1972), Vol. 8.
- [3] J.R. Taylor, Nuovo Cimento **B23**, 313 (1974).
- [4] M.D. Semon and J.R. Taylor, Nuovo Cimento **A26**, 48 (1975).
- [5] E. O. Alt, W. Sandhas, and H. Ziegelmann, Phys. Rev. **C 17**, 1981 (1978).
- [6] H. Witała, J. Golak, R. Skibiński, and W. Glöckle, in preparation
- [7] W.F. Ford, Phys. Rev. **133**, B1616 (1964).
- [8] W.F. Ford, J. Math. Phys. **7**, 626 (1966).
- [9] L.P. Kok and H. van Haeringen, Phys. Rev. **C21**, 512 (1980).
- [10] W. Glöckle, The Quantum Mechanical Few-Body Problem, Springer Verlag 1983.
- [11] W. Glöckle, H. Witała, D. Hüber, H. Kamada, J. Golak, Phys. Rep. **274**, 107 (1996).
- [12] M. Yamaguchi, H. Kamada, and Y. Koike, Prog. Theor. Phys. **114**, 1323 (2005)
- [13] Ch. Elster, J.H. Thomas, and W. Glöckle, Few-Body Systems **24**, 55 (1998).
- [14] Handbook of mathematical functions, ed. M. Abramowitz and I. A. Stegun, Dover Publ., N. Y. 1972.
- [15] Numerical Recipes: the art of scientific computing, W.H. Press, S.A. Teukolsky, W.T. Vetterling, B.P. Flannery, Cambridge University Press 2007.
- [16] L.P. Kok and H. van Haeringen, Phys. Rev. Lett. **46**, 1257, (1981).
- [17] H. van Haeringen, Charged Particle Interactions, Theory and Formulas, Coulomb Press Leyden, 1985.
- [18] R. Machleidt, F. Sammarruca, and Y. Song, Phys. Rev. **C53**, R1483 (1996).

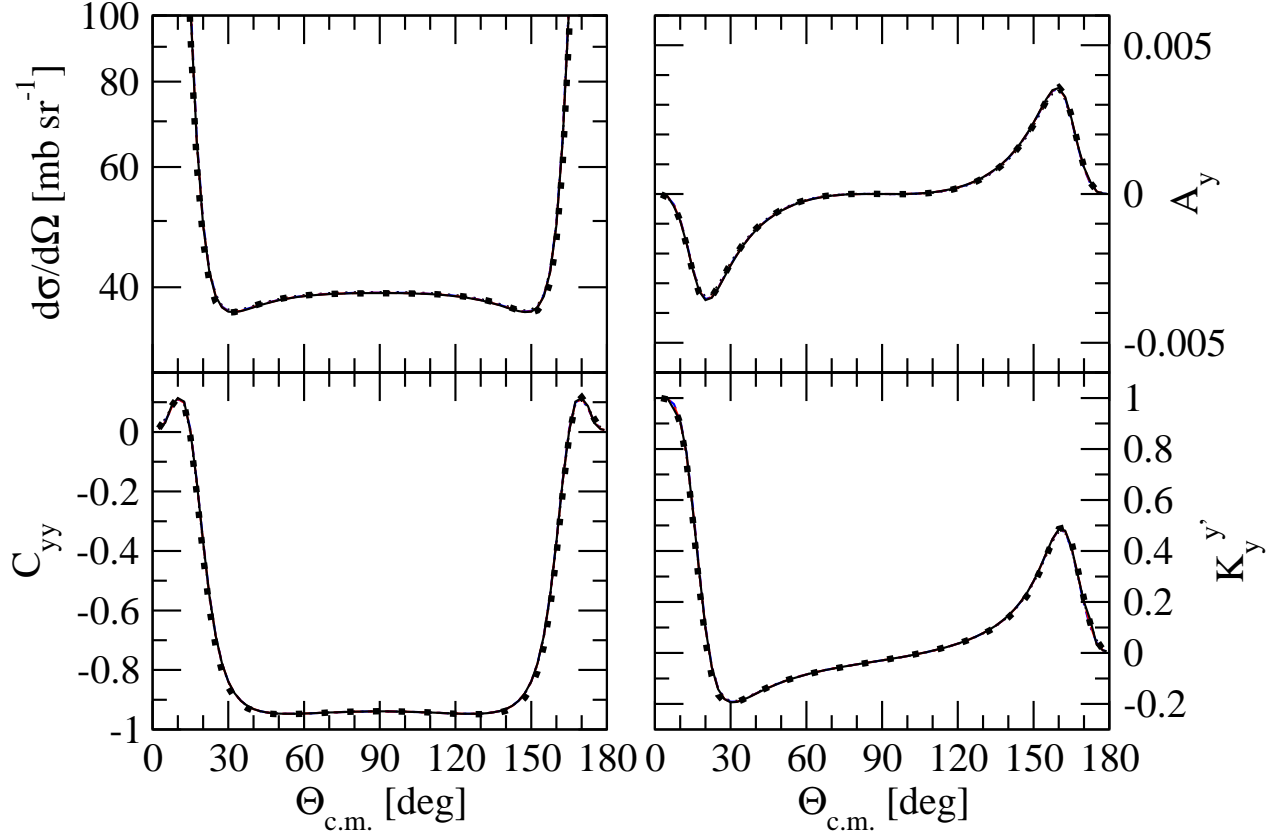


FIG. 1: (color online) The convergence of the pp scattering cross section ($\frac{d\sigma}{d\Omega}$), analyzing power (A_y), spin correlation coefficient (C_{yy}), and spin transfer coefficient (K_y^y) at $E_p^{\text{lab}} = 13$ MeV as a function of the c.m. scattering angle calculated with the screened Coulomb force and the CD Bonn nucleon-nucleon potential [18], which is kept for the partial waves up to $j \leq 3$. The screening radius is $R = 120$ fm and $n = 1$ (dotted line), $n = 2$ (dashed-dotted line), $n = 3$ (dashed line), and $n = 4$ (solid line). The curves for $n = 1$ to $n = 4$ all overlap on the scale of the figure. The exact Vincent-Phatak result is given by thick dots.

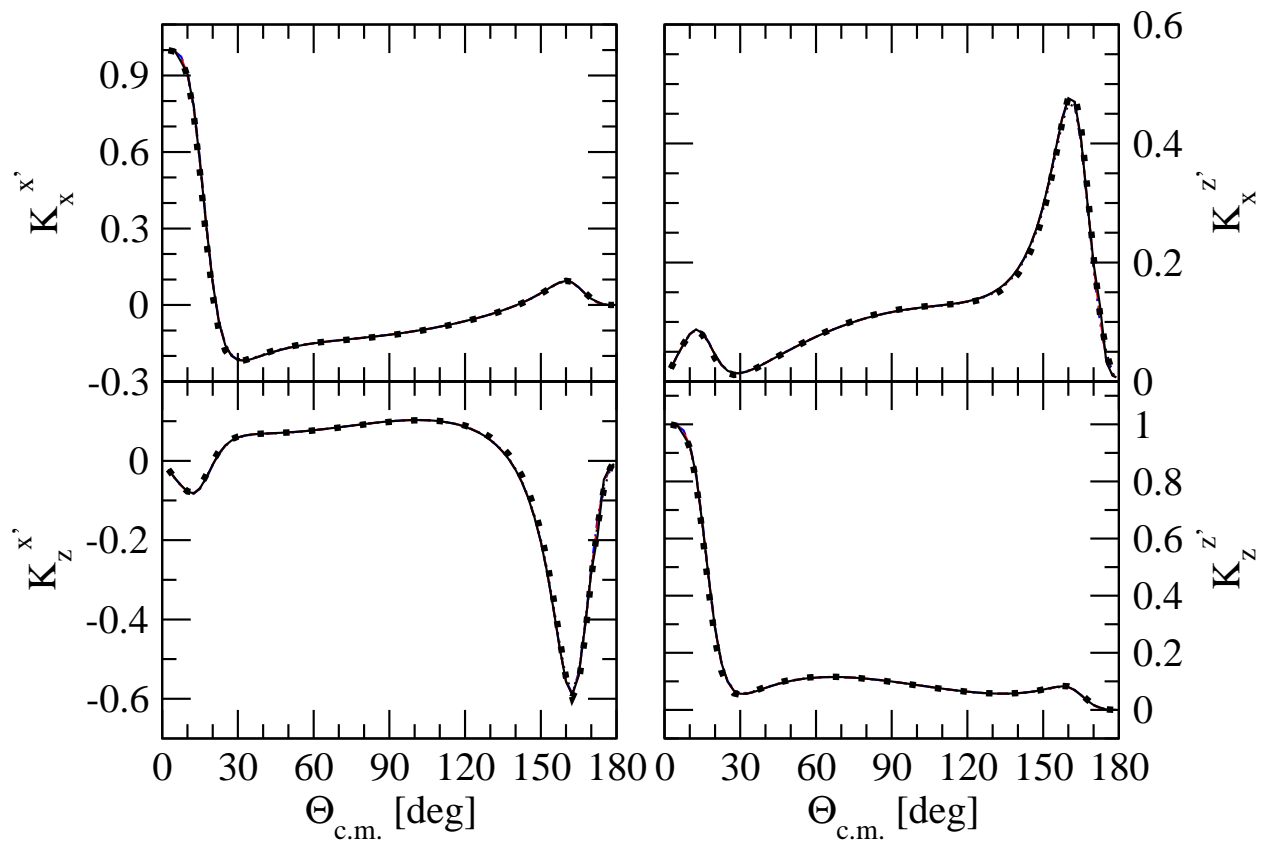


FIG. 2: (color online) The same as in Fig.1 but for other pp scattering spin transfer coefficients.

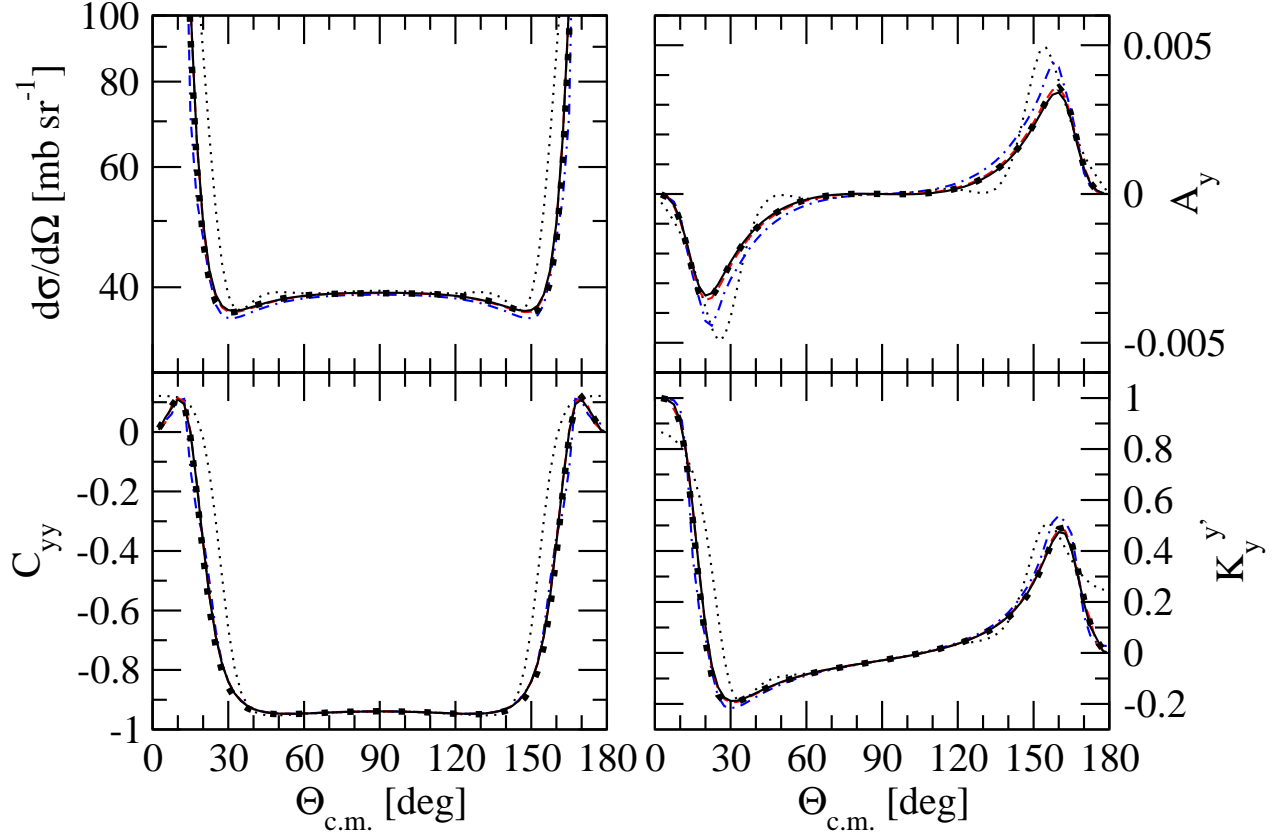


FIG. 3: (color online) The pp scattering cross section ($\frac{d\sigma}{d\Omega}$), analyzing power (A_y), spin correlation coefficient (C_{yy}), and spin transfer coefficient (K_y') at $E_p^{\text{lab}} = 13$ MeV as a function of the c.m. scattering angle calculated with the screened Coulomb force and the CD Bonn nucleon-nucleon potential [18], which is kept for the partial waves up to $j \leq 3$. The screened results are for $n = 4$ and different values of the screening radius R : $R = 20$ fm (dotted line), $R = 60$ fm (dashed-dotted line), $R = 120$ fm (dashed line), and $R = 180$ fm (solid line). The thick dots are the Vincent-Phatak's exact results.

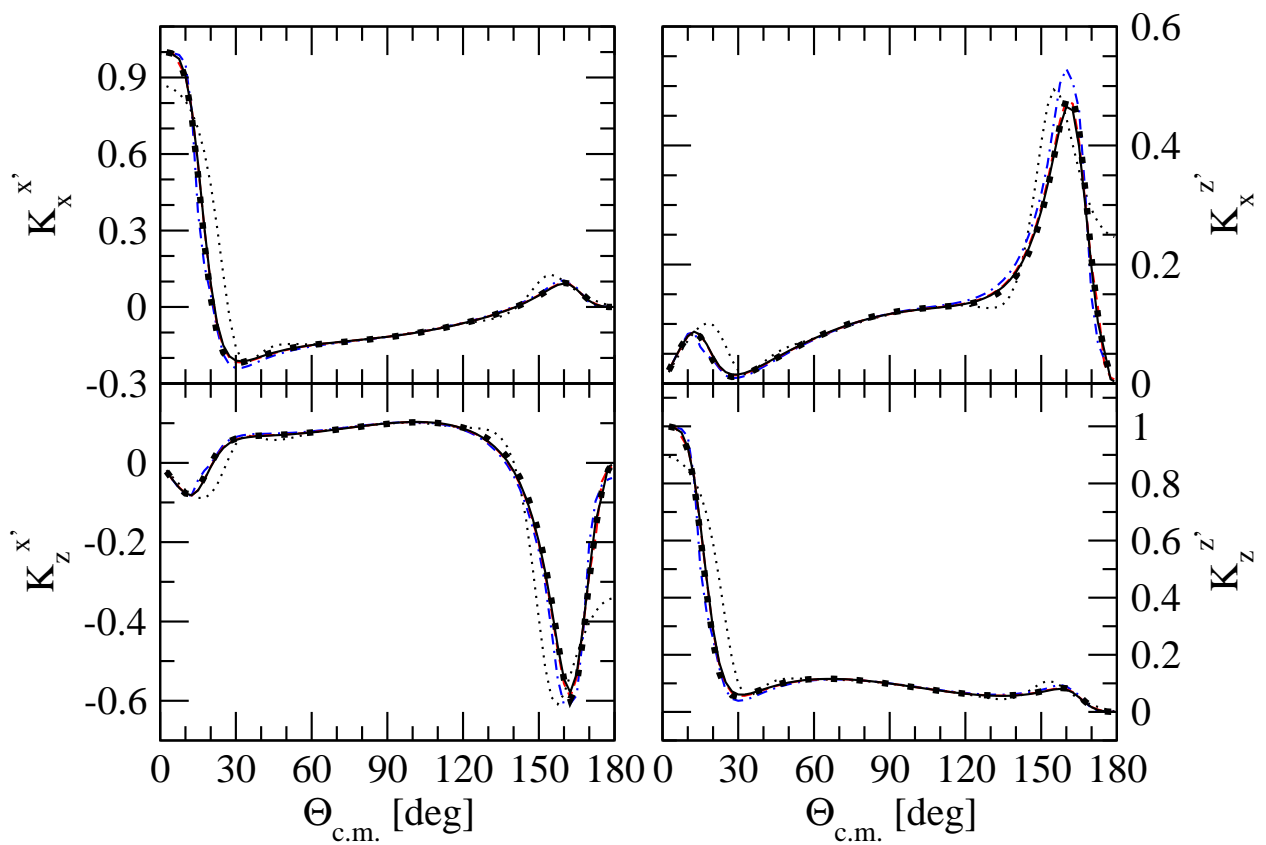


FIG. 4: (color online) The same as in Fig. 3 for other spin transfer coefficients.

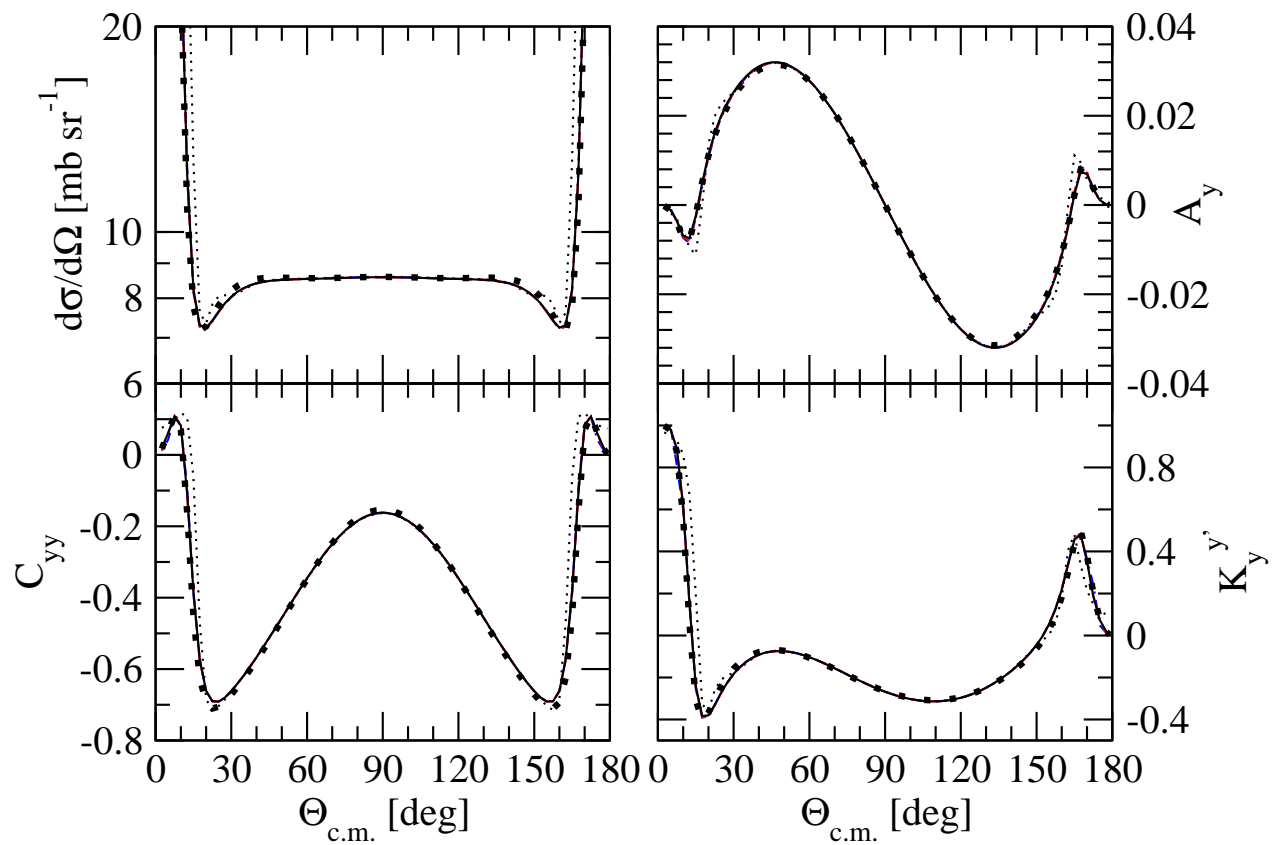


FIG. 5: (color online) The same as in Fig.3 at $E_p^{lab} = 50$ MeV.

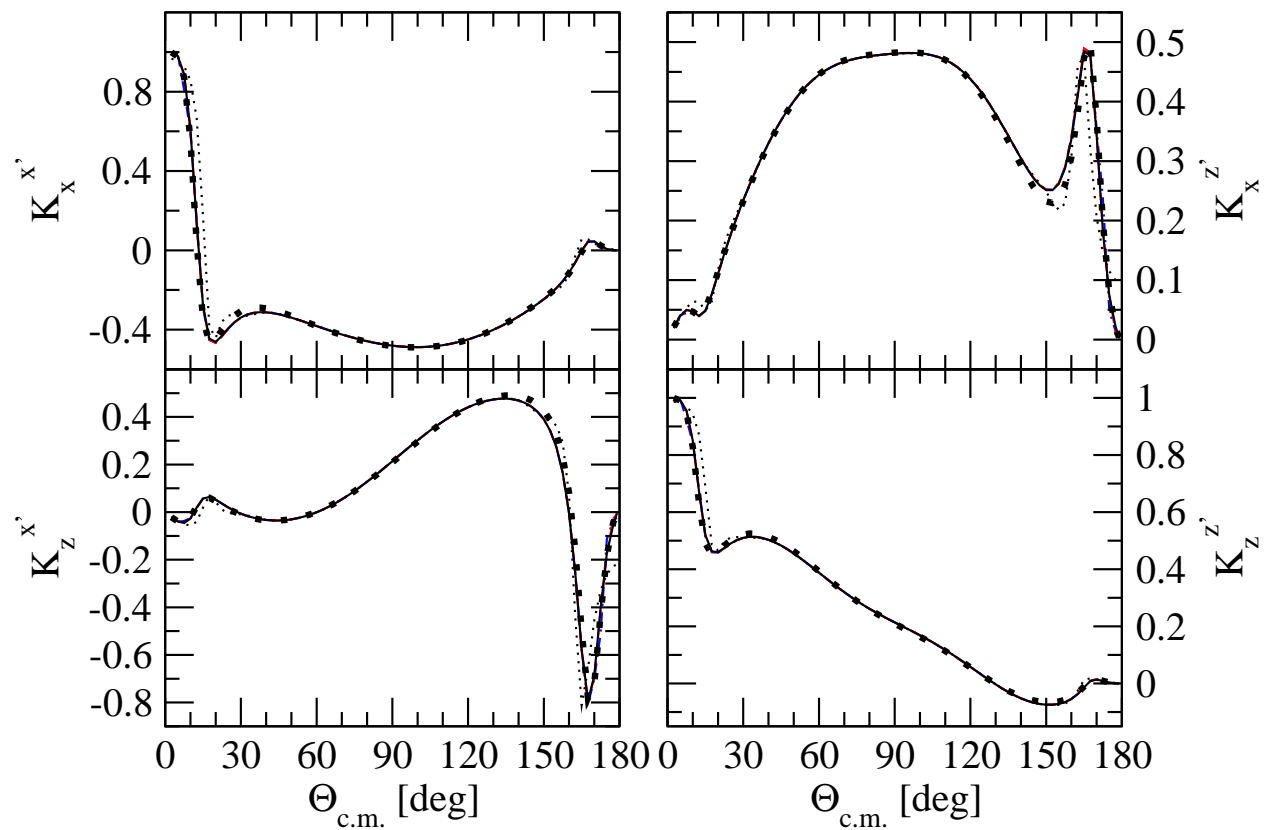


FIG. 6: (color online) The same as in Fig.4 at $E_p^{lab} = 50$ MeV.

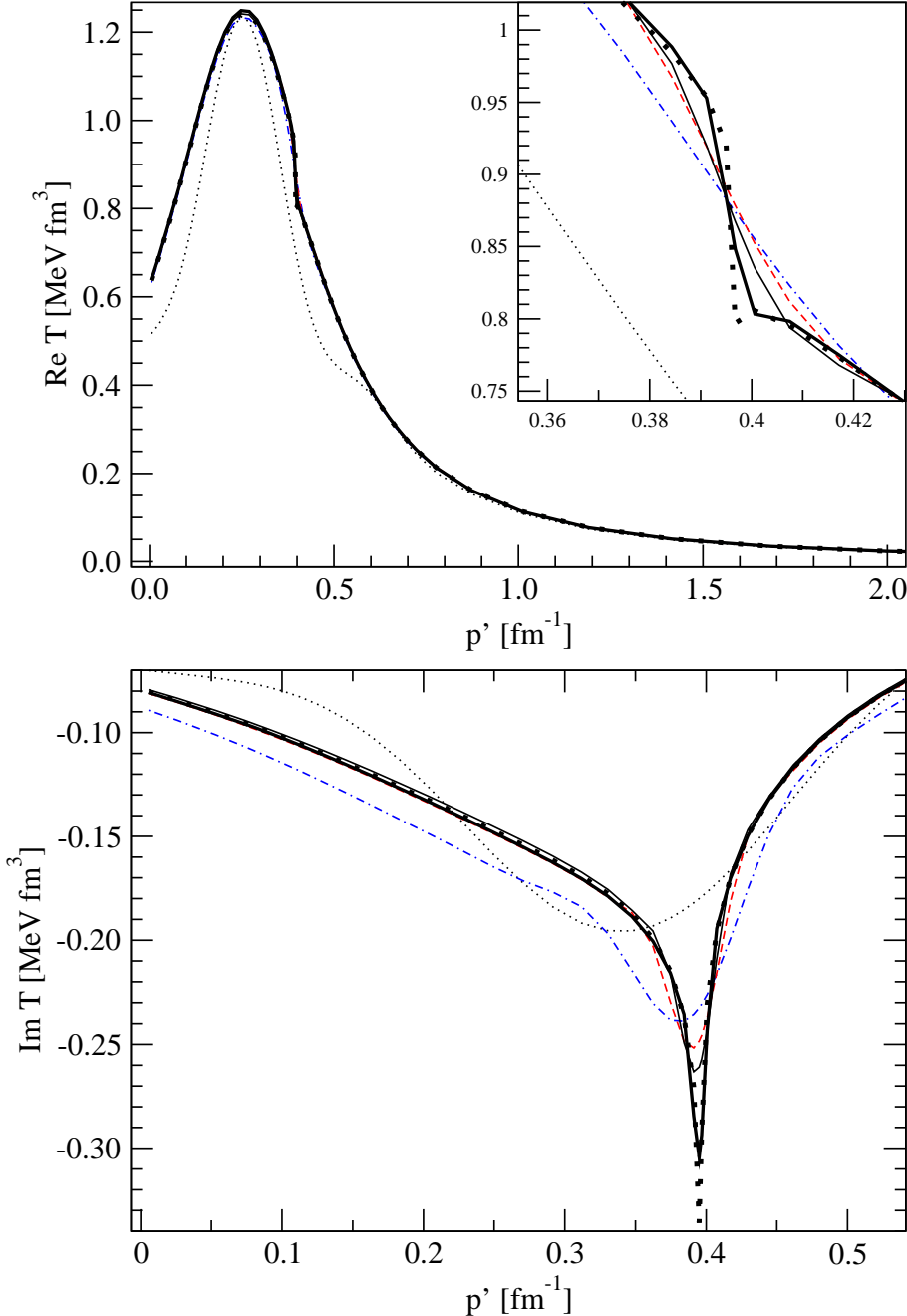


FIG. 7: (color online) Limiting behaviour of the real (upper) and the imaginary (lower) parts of the off-the-energy-shell screened t-matrix $t_c^R(p, p', x)$ at $E_p^{lab} = 13$ MeV, $p = 0.36$ fm $^{-1}$, and $x = 0.71$ as a function of the p' momentum for $n = 4$ and different values of the screening radius R : $R = 20$ fm (dotted line), $R = 60$ fm (dashed-dotted line), $R = 120$ fm (dashed line), $R = 180$ fm (thin solid line), $R = 500$ fm (thick solid line). The pure Coulomb off-shell result of Eq.(15) is given by thick dots. The half-shell situation is reached at $p' = k = \sqrt{m_p E_{c.m.}} = 0.396$ fm $^{-1}$. In the insert a discontinuity develops if p' approaches k from below or above (see text).

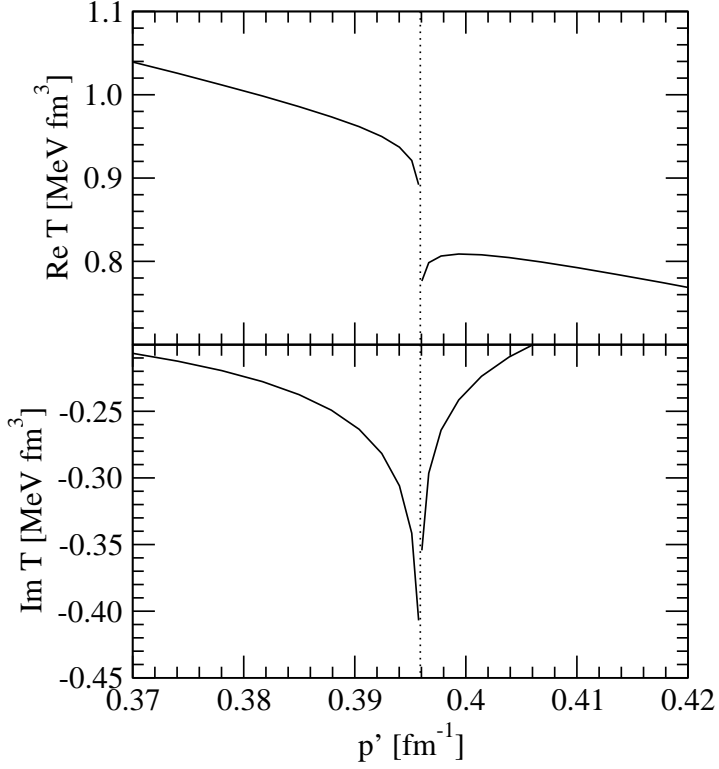


FIG. 8: The discontinuity of the real (upper row) and the imaginary (lower row) parts of the off-the-energy-shell pure Coulomb t-matrix $t_c(p, p', x)$ (given by Eq.(16)) near $p' = k = \sqrt{m_p E_{c.m.}} = 0.396 \text{ fm}^{-1}$ at $E_p^{lab} = 13 \text{ MeV}$, $p = 0.361 \text{ fm}^{-1}$, and $x = 0.71$ as a function of the p' momentum.

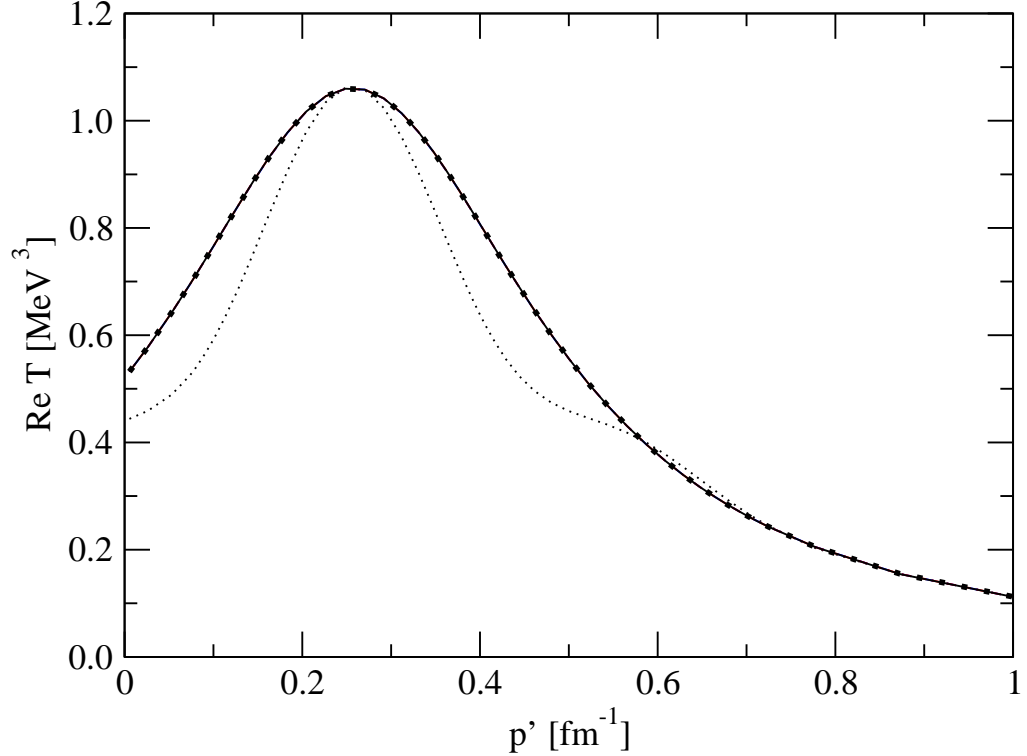


FIG. 9: (color online) Limiting behaviour of the real part of the off-the-energy-shell screened t-matrix $t_c^R(p, p', x)$ at negative energy $E = -13$ MeV, $p = 0.36$ fm $^{-1}$, and $x = 0.71$, as a function of the p' momentum for $n = 4$ and different values of the screening radius R : $R = 20$ fm (dotted line), $R = 60$ fm (dashed-dotted line), $R = 120$ fm (dashed line), and $R = 180$ fm (solid line). The pure Coulomb off-shell result of Eq.(15) is given by thick dots.

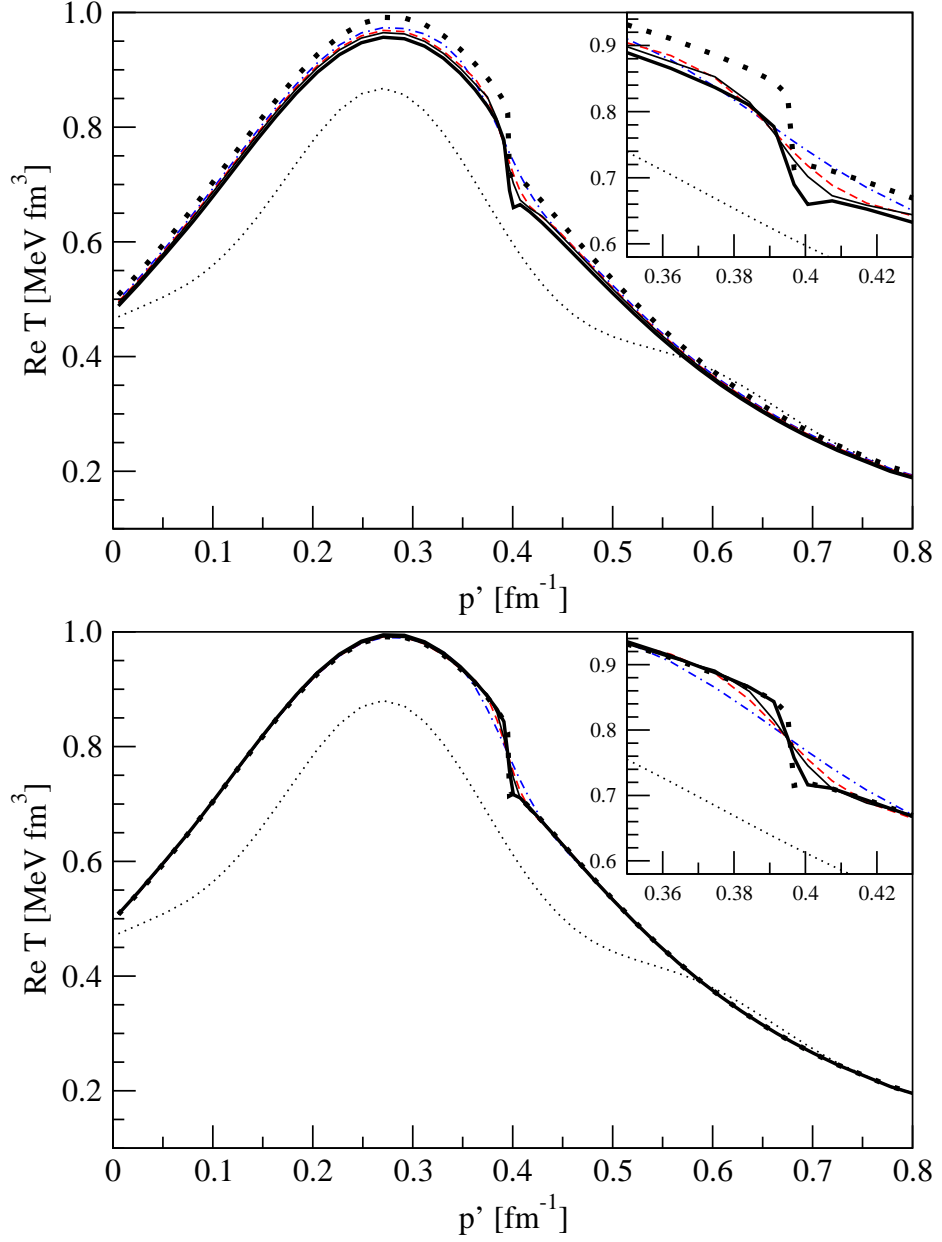


FIG. 10: (color online) The real part of the half-the-energy-shell screened t-matrix $t_c^R(p, p, x)$ before (upper row) and after (lower row) the renormalization. The proton lab. energy is $E = 13$ MeV, and $x = 0.71$. The screening potential was taken with $n = 4$ and different values of the screening radius R : $R = 20$ fm (dotted line), $R = 60$ fm (dashed-dotted line), $R = 120$ fm (dashed line), $R = 180$ fm (solid line) and $R = 500$ fm (thick solid line) The pure Coulomb half-shell result of Eq.(17) is given by thick dots.

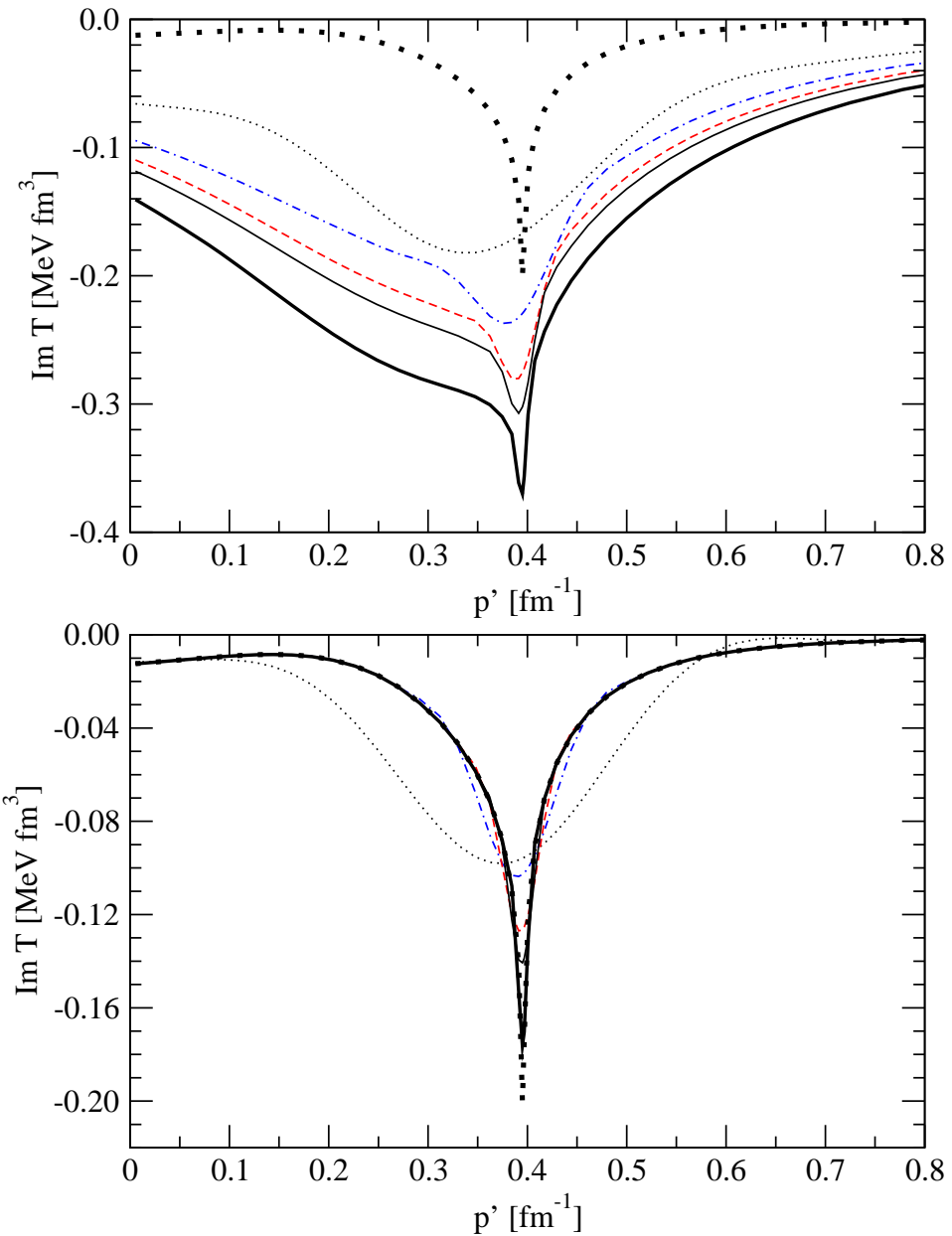


FIG. 11: (color online) The same as in Fig. 10 but for imaginary part of the half-the-energy-shell t-matrix.

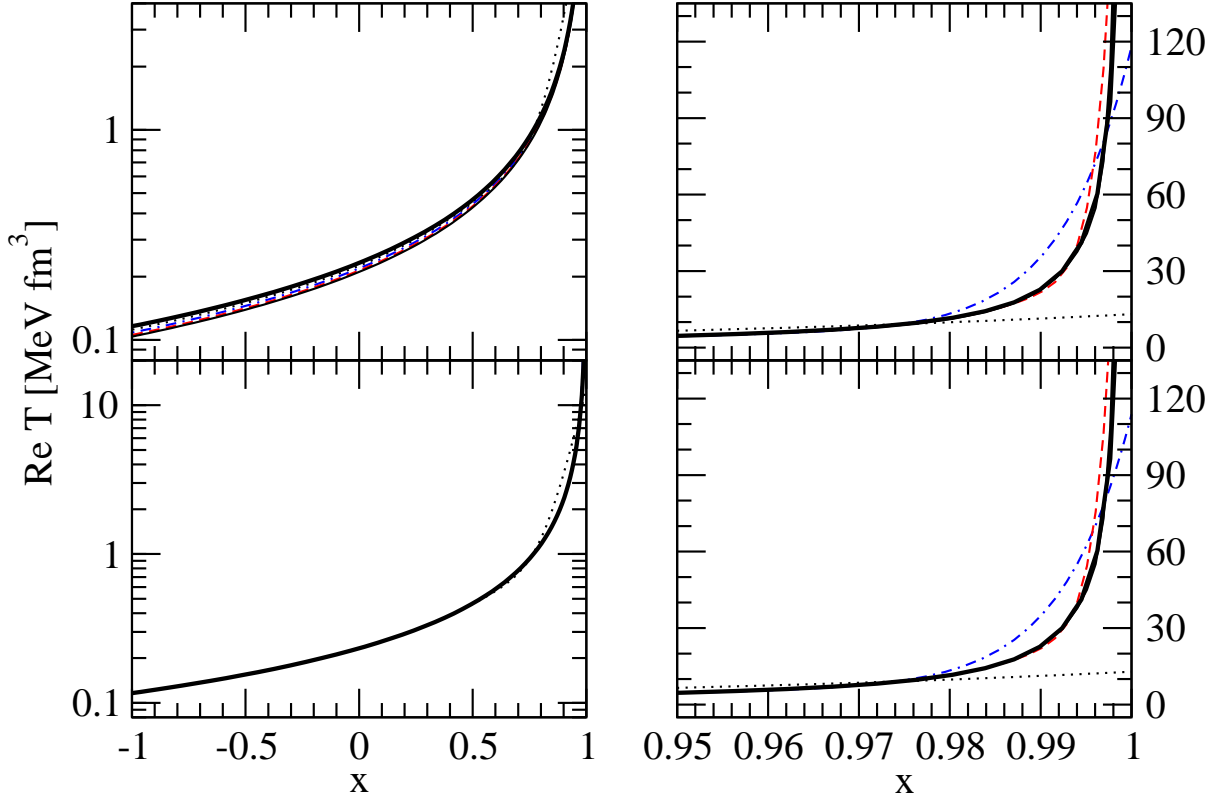


FIG. 12: (color online) The real part of the on-the-energy-shell screened t-matrix $t_c^R(p, p, x)$ (upper row) and the corresponding renormalized t-matrices (lower row) at $E_p^{lab} = 13$ MeV as a function of x for $n = 3$ and different values of the screening radius R : $R = 20$ fm (dotted line), $R = 60$ fm (dashed-dotted line), $R = 120$ fm (dashed line), $R = 180$ fm (thin solid line). The Coulomb on-shell amplitude of Eq.(18) is given by thick solid line. The left and the right column differs only in the scale of the x-axis.

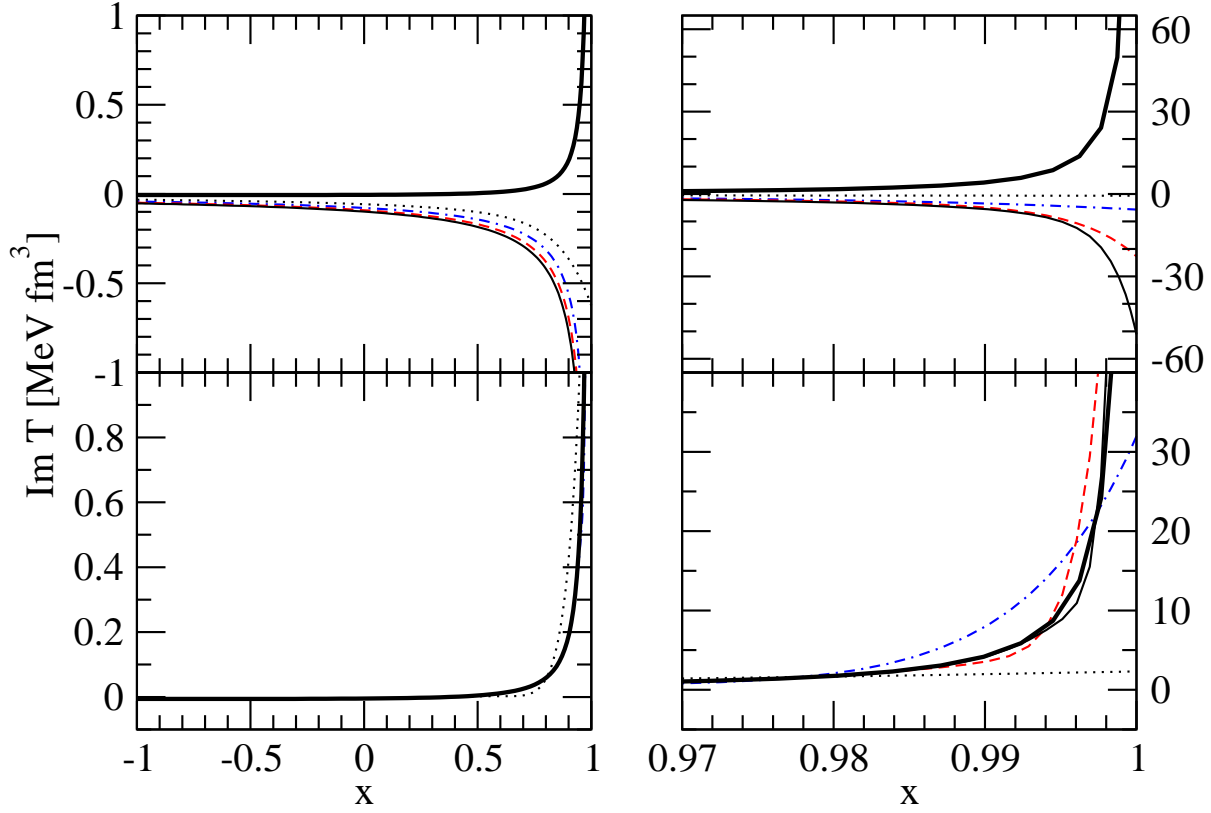


FIG. 13: (color online) The imaginary part of the on-the-energy-shell screened t-matrix $t_c^R(p, p, x)$ (upper row) and the corresponding renormalized t-matrices (lower row) at $E_p^{lab} = 13$ MeV as a function of x for $n = 3$ and different values of the screening radius R . For the description of lines see Fig.12.